The Astronomical Journal, 144:47 (11pp), 2012 August doi:10.1088/0004-6256/144/2/47

THE ROAD TO THE RED SEQUENCE: A DETAILED VIEW OF THE FORMATION OF A MASSIVE GALAXY AT $z \sim 2$

Ignacio Ferreras[1], Anna Pasquali[2], Sadegh Khochfar[3], Harald Kuntschner[4], Martin Kümmel[4], Nor Pirzkal[5], Rogier Windhorst[6], Sangeeta Malhotra[6], James Rhoads[6], Robert W. O'Connell[7], Seth Cohen[6], Nimish P. Hathi[8], Russell E. Ryan, Jr.[9], and Haojing Yan[10]

[1] Mullard Space Science Laboratory, University College London, Holmbury St Mary, Dorking, Surrey RH5 6NT, UK; ferreras@star.ucl.ac.uk
[2] Astronomisches Rechen Institut, Zentrum für Astronomie der Universität Heidelberg, Mönchhofstrasse 12–14, 69120 Heidelberg, Germany
[3] Theoretical Modelling of Cosmic Structures Group, Max-Planck-Institut für Extraterrestrische Physik, Giessenbachstr., D-85748 Garching, Germany
[4] European Southern Observatory, Karl-Schwarzschild-Str. 2, D-85748 Garching, Germany
[5] Space Telescope Science Institute, 3700 San Martin Drive, Baltimore, MD 21218, USA
[6] Department of Physics and Astronomy, Arizona State University, P.O. Box 871504, Tempe, AZ 85287-1504, USA
[7] Department of Astronomy, University of Virginia, Charlottesville, VA 22904-4325, USA
[8] Observatories of the Carnegie Institute of Washington, Pasadena, CA 91101, USA
[9] Physics Department, University of California, Davis, CA 95616, USA
[10] Department of Physics and Astronomy, University of Missouri, Columbia, MO 65211, USA
Received 2011 December 17; accepted 2012 May 23; published 2012 July 6

ABSTRACT

Over half of the census of massive galaxies at $z \sim 2$ are dominated by quiescent stellar populations. The formation mechanism for these galaxies is still under debate, with models relying either on massive and early mergers or cold accretion. It is therefore imperative to understand in detail the properties of these galaxies. We present here a detailed analysis of the star formation history (SFH) of FW4871, a massive galaxy at $z = 1.893 \pm 0.002$. We compare rest-frame optical and NUV slitless grism spectra from the *Hubble Space Telescope* with a large set of composite stellar populations to constrain the underlying SFH. Even though the morphology features prominent tidal tails, indicative of a recent merger, there is no sign of ongoing star formation within an aperture encircling one effective radius, which corresponds to a physical extent of 2.6 kpc. A model assuming truncation of an otherwise constant SFH gives a formation epoch $z_F \sim 10$ with a truncation after 2.7 Gyr, giving a mass-weighted age of 1.5 Gyr and a stellar mass of (0.8–3) $\times 10^{11}$ $M_\odot$ (the intervals representing the output from different population synthesis models), implying star formation rates of 30–110 $M_\odot$ yr^{-1}. A more complex model including a recent burst of star formation places the age of the youngest component at 145^{+450}_{-70} Myr, with a mass contribution lower than 20%, and a maximum amount of dust reddening of $E(B-V) < 0.4$ mag (95% confidence levels). This low level of dust reddening is consistent with the low emission observed at 24 μm, corresponding to rest-frame 8 μm, where polycyclic aromatic hydrocarbon emission should contribute significantly if a strong formation episode were present. The color profile of FW4871 does not suggest a significant radial trend in the properties of the stellar populations out to 3 R_e. We suggest that the recent merger that formed FW4871 is responsible for the quenching of its star formation.

Key words: galaxies: elliptical and lenticular, cD – galaxies: individual (FW4871) – galaxies: stellar content

Online-only material: color figures

1. INTRODUCTION

The formation of the most massive galaxies remains one of the main challenges of galaxy formation models. Within the observed bimodality of the galaxy population (e.g., Kauffmann et al. 2003; Baldry et al. 2004), massive galaxies dominate the so-called red sequence, which features mostly old, passively evolving stellar populations, suggesting an early, short-lived period of star formation. The implied rapid and efficient star formation history (SFH) is corroborated by the presence of massive galaxies at $z \sim 1$–3 (Cimatti et al. 2008; Pérez-González et al. 2008) and by the mild evolution with redshift of the corresponding comoving number density (Fontana et al. 2006; Conselice et al. 2007; Ferreras et al. 2009a; Banerji et al. 2010). On the other hand, the strong evolution with redshift found on the mass–size plane (e.g., Daddi et al. 2005; Trujillo et al. 2006; Longhetti et al. 2007; van Dokkum et al. 2008) remains an open question, with ongoing arguments debating whether the main size growth scenario at $z \lesssim 2$ is due to either the emergence of early-type galaxies with cosmic time, or to intrinsic mechanisms involving gas ejecta, minor mergers, or major mergers (e.g., Khochfar & Silk 2006b; Bournaud et al. 2007; Fan et al. 2008; Damjanov et al. 2009; van der Wel et al. 2009; Naab et al. 2009; Shankar et al. 2010), although see Ragone-Figueroa & Granato (2011) and Trujillo et al. (2011) for a criticism of the gas expulsion scenario. The observed size–mass evolution of massive galaxies has resulted in a major revision of our understanding of galaxy growth (see, e.g., Nair et al. 2011).

It is believed that two main channels of galaxy growth are important under the hierarchical formation paradigm: one driven by shock heating and subsequent cooling of the gas in halos (White & Rees 1978) and another one driven by the accretion of cold gas along narrow filaments that does not shock heat (Dekel & Birnboim 2006; Dekel et al. 2009; Kereš et al. 2009). At redshifts $z \gtrsim 2$, the presence of massive galaxies already in place suggests that a very efficient mechanism must operate to fuel and transform vast amounts of gas into stars within a dynamical time.

Wide, nearby surveys along with deep surveys complemented by high-resolution imaging are opening this important issue to

scrutiny. In the past, the properties of the stellar populations of $z \gtrsim 1$ galaxies relied on photometric measurements or low signal-to-noise (S/N) spectra, mainly targeting the rest-frame NUV (see, e.g., Spinrad et al. 1997), with the inherent degeneracies (Ferreras & Yi 2004). The advent of the Wide Field Camera 3 on board the *Hubble Space Telescope* (*HST*) has opened up an important spectral window. With its IR slitless grisms (G102 and G141) it is possible to target the Balmer break region of massive galaxies over a redshift range ($1.5 < z < 3$) where our standard ideas of galaxy growth can be put to the test.

We present here a detailed analysis of the SFH of a massive galaxy at $z \sim 2$, discovered in the *HST*/Wide Field Camera 3 (WFC3) Early Release Science (ERS) by van Dokkum & Brammer (2010). The slitless grism data from WFC3-IR have allowed us to probe in detail the star formation process of a massive galaxy caught in its final merging stages toward the red sequence. The age of the universe at that redshift (around 3.4 Gyr) enables us to constrain in more detail the age distribution. We explore a large range of plausible SFHs, with the aim of estimating an upper bound to the recent and sustained star formation rate for this galaxy, an issue that will shed light on the main processes contributing to the growth of massive galaxies. In contrast to van Dokkum & Brammer (2010), our paper uses the latest flux calibration available for the WFC3 grisms, a very important issue when extracting SFHs from spectral fitting. Furthermore, we explore a huge volume of parameter space, instead of a few trial SFHs, to determine not only the best fits, but robust uncertainties. In addition, we compare two different sets of population synthesis models to assess the systematics.

In this paper we assume a standard ΛCDM cosmology with $H_0 = 70$ km s^{-1} Mpc^{-1}, and $\Omega_m = 0.3$. All magnitudes are given in the AB photometric system.

2. LOOKING FOR PASSIVE GALAXIES WITH A SLITLESS GRISM

Following up our previous work on the spectral analysis of massive galaxies at moderate-to-high redshift, we searched the WFC3/ERS slitless grism data set, looking for galaxies with a prominent Balmer break. This technique has allowed us to constrain the SFH of early-type galaxies out to $z \sim 1.2$ in the HUDF (Pasquali et al. 2006) and the wider *HST*/ACS coverage of the GOODS North and South fields (Ferreras et al. 2009b). The IR coverage of WFC3 enables us to probe the very sensitive region around the Balmer break at higher redshifts.

We searched through the data available from the ERS programme for WFC3, ID 11359 (PI: O'Connell). A field centered at R.A. = 03:32:17.6 and decl. = −27:42:32.4 (J2000) was imaged with an exposure time of 5017.6 s in each of the WFC3/IR F098M, F125W, and F160W filters. The data were reduced with the standard WFC3 pipeline. Slitless spectroscopy of the same field was obtained through the WFC3/IR G102 (*J* band) and G141 (*H* band) grisms, for a total exposure time of 4211.7 s per grism. The grism spectra were reduced with the aXe 2.1 software[11] (Kümmel et al. 2010). The data cover a field of view of 4.65 arcmin^2 (see Straughn et al. 2011 for details) with a spectral coverage of 0.8–1.6 μm and resolution between $R = 210$ at $\lambda = 1\,\mu$m and $R = 130$ at 1.4 μm. The spectral coverage allows us to probe the Balmer break in the redshift window $1 < z < 3$, although the shallowness of the ERS data restricts this range to $z \lesssim 2$ for the case of massive ($M_s \gtrsim 10^{11}\ M_\odot$) galaxies, where M_s is the stellar mass.

From this data set, we found only one galaxy with a high enough S/N for the application of our methodology to extract SFHs. This galaxy has been already presented in van Dokkum & Brammer (2010) and identified as FW4871 from the FIREWORKS catalog (Wuyts et al. 2008). In this paper we look in detail at the constraints one can impose on its stellar populations, employing a vast range of SFHs.

To further constrain the models, we also extracted the observed-frame optical spectrum of FW4871 from the 2005 observations with the Advanced Camera for Surveys (ACS) through its WFC/G800L grism, as part of the program Probing Evolution And Reionization Spectroscopically (ID 10530, PI: Malhotra). The total exposure time was 15,140 s, and the spectrum was extracted and calibrated with the aXe software (Kümmel et al. 2009).

In order to avoid contamination from a nearby source in the grism images, we have extracted two optical+IR spectra for FW4871, over apertures of three and five pixels on the WFC3-IR grism data, corresponding to diameters of 0.38 and 0.64 arcsec, respectively. The IR G102 spectra have been degraded to the same spectral resolution of those acquired with G141 ($R = 130$ at 1.4 μm). The original spectral resolution of the ACS spectra is preserved, since these data will be fitted independently of the IR data. Figure 1 shows both ACS and WFC3 spectra within these two apertures. The S/N (mid panels) is high enough for a detailed analysis of the stellar populations (Section 4). Note the lack of strong emission lines ([O II], Hβ, and [O III] fall within the wavelength coverage of the WFC3 data) and the presence of prominent Balmer lines, typical of stellar populations that underwent a recent period of star formation, i.e., a k+a galaxy (Dressler & Gunn 1992).

The spectral fitting method requires knowledge of the effective spectral resolution. We matched a set of simple stellar populations (SSPs) with similar absorption lines (around an age of 1 Gyr) against the data, and smoothed the spectra using a Gaussian kernel with variable width. We also explored a range of redshifts for an accurate estimate. We refined the redshift estimate from $z = 1.902$ in van Dokkum & Brammer (2010) to $z = 1.893$, and obtained an effective resolution FWHM of 120 Å, in agreement with the expected resolution of G141 ($R = 130$ at 1.4 μm). We note that the spectral resolution of slitless grism spectroscopy is strongly affected by object size. The galaxy presented in this paper is, of course, resolved, which implies a lower spectral resolution than the camera specification values, given for unresolved sources.

3. INTRINSIC COLOR PROFILE

In addition to the spectroscopic data, we make use of the NIR images from WFC3/ERS (Windhorst et al. 2011). Imaging through three passbands is available: F098M, F125W, and F160W, reaching a 50% point-source completeness limits of AB(F098M) = 27.2 mag, AB(F125W) = 27.5 mag, and AB(F160W) = 27.2 mag, at the 5σ level (Windhorst et al. 2011). At the redshift of our target, these three passbands closely map rest-frame *U*, *B*, and *V* standard filters. We ran a set of SSPs from the latest versions of the Bruzual & Charlot (2003) models to determine the *K*-corrections relating these observed and rest-frame filters. As expected, the *K*-corrections are rather low, always below 0.05 mag even if the metallicity is unknown over one decade.

[11] http://axe.stsci.edu/axe/index.html

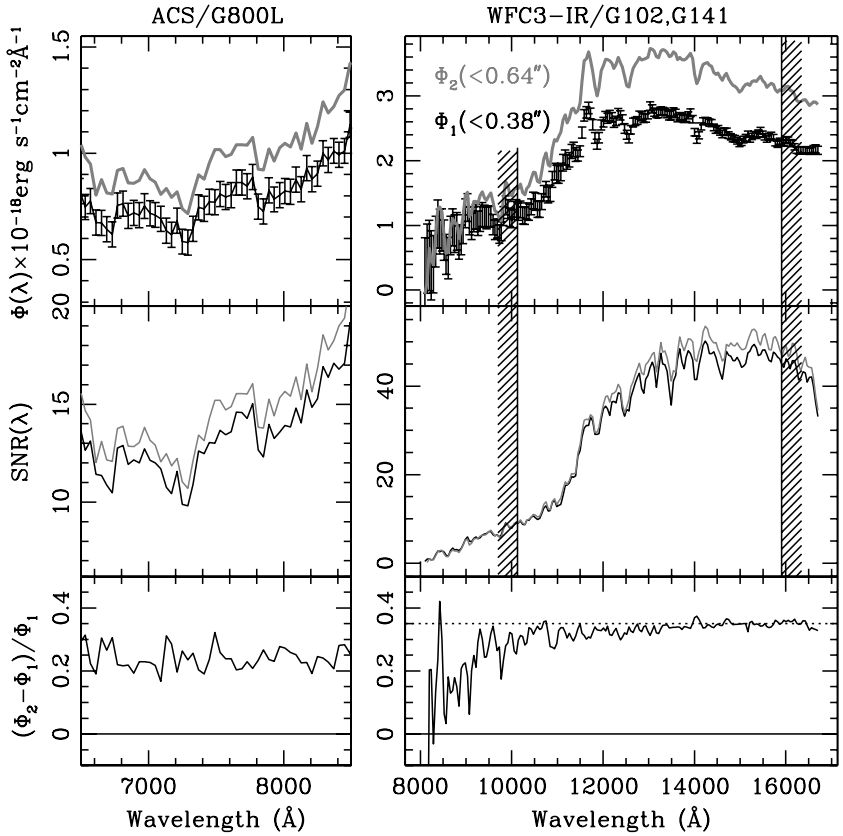

Figure 1. Slitless grism spectra of galaxy FW4871 from the Advanced Camera for Surveys (left) and the Wide Field Camera 3-IR (right). Two extractions are used in the analysis (wider extractions would include flux from a neighboring object). The three panels, from top to bottom, show the flux, including error bars for the 0.38 arcsec extraction; S/N; and flux ratio between the extractions. The vertical shaded regions give the fitting interval for the analysis of the stellar populations.

Table 1
Observations (AB Magnitudes, Errors Given at the 1σ Level)

Redshift	F160W[a]	$R_e(''$)	n_S	Aperture	F098M–F160W[b]	F125W–F160W[b]	MgUV[b,c]	D4000[d]
1.893 ± 0.002	19.81 ± 0.07	0.31 ± 0.04	5.4 ± 1.1	0.″38	1.89 ± 0.34	0.35 ± 0.22	1.16 ± 0.04	1.314 ± 0.013
				0.″64	1.88 ± 0.26	0.40 ± 0.16	1.15 ± 0.05	1.297 ± 0.012

Notes.
[a] Total apparent magnitude corresponding to the Sérsic fit.
[b] Measured within the apertures (given as diameters).
[c] As defined in Daddi et al. (2005).
[d] As defined in Balogh et al. (1999).

In order to constrain the surface brightness profile of the galaxy, we ran GALFIT (Peng et al. 2010) on the three WFC3/IR images, for a Sérsic profile plus a constant sky background. The point spread function (PSF) is built from a set of 11 stars extracted from the same images. The results are given in Table 1, where the uncertainties are quoted at the 1σ level and are computed from a set of GALFIT runs on the same images, replacing the combined image of the PSF by those from the individual stars. The half-light radius (0.31 ± 0.04 arcsec) maps into a projected physical distance of 2.64 ± 0.35 kpc at the redshift of FW4871, which makes this object a typical example of the compact massive galaxies found at similar redshift (e.g., Daddi et al. 2005; Trujillo et al. 2006; van Dokkum et al. 2008), although we note that the CM05 models would locate this galaxy closer to the local sample on the mass–size plane (see below). The two extractions of the spectra we will use for the analysis roughly correspond to apertures with diameter 0.″38 and 0.″64, hence enclosing $R_e/2$ and R_e, respectively. The high value of the Sérsic index makes the surface brightness profile compatible with an early-type morphology.

In order to determine the intrinsic color gradient of FW4871, we follow the approach described in Ferreras et al. (2005) involving a Voronoi tessellation to increase the S/N of the image, preserving as much as possible the spatial information. Figure 2 shows the original frames (left), and a deconvolved reconstruction (right), using the *lucy* task in IRAF (Lucy 1974). The figure uses all three NIR passbands to generate an RGB color image. This galaxy reveals itself as a major merging event, with nearby objects displaying tidal features as well, most notably the galaxy to the NW, at the same redshift, identified as FW4887, a galaxy with a mass $\sim 1/10$ of FW4871, which will likely contribute to a later minor merger with FW4871 (van Dokkum & Brammer 2010). The spiral-like shape of the tails might alternatively suggest a late-type galaxy morphology.

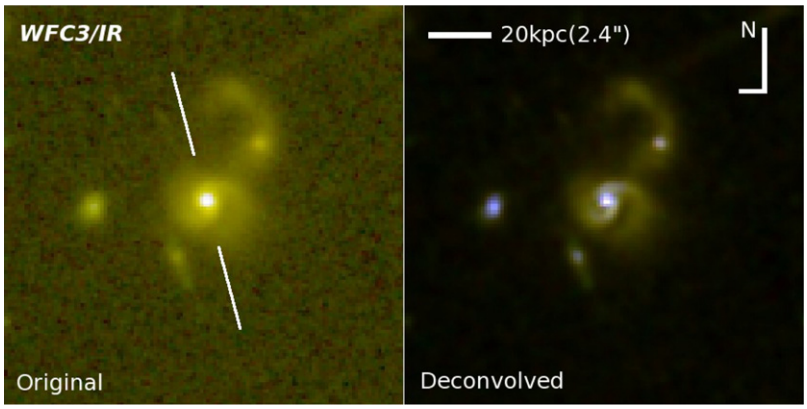

Figure 2. Color montage of FW4871 using WFC3/IR images in the F098M (blue), F125W (green), and F160W (red) passbands. The panels illustrate the effect of the deconvolution. Note the nearby distorted galaxy located NW of FW4871 is a companion (identified as FW4887; van Dokkum & Brammer 2010). The orientation of the extraction of the spectrum is shown as two white segments in the left-hand panel.

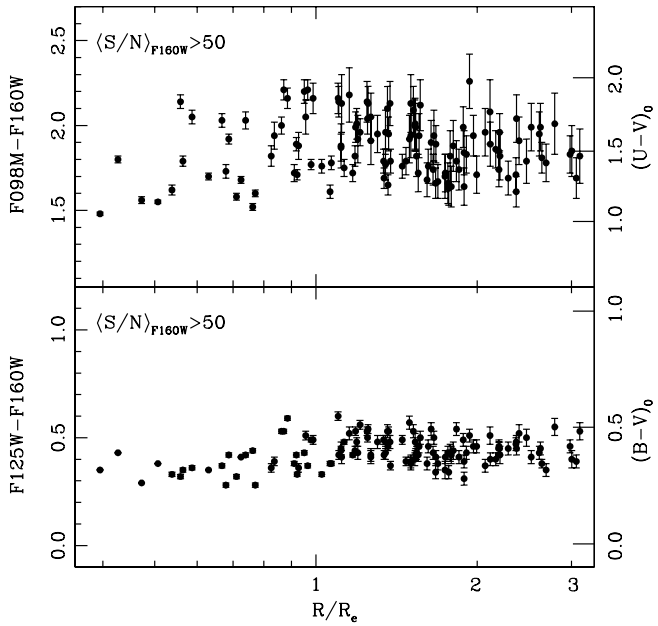

Figure 3. Color profile after a Voronoi tessellation of the WFC3/IR images. The tessellation is performed with a target S/N per bin in the F160W passband above 50. The right axes give the K-corrected, rest-frame $U - V$ (top) and $B - V$ colors.

However, as we will show below, the lack of dust and ongoing star formation from the analysis of the spectra makes this option unlikely.

The Voronoi tessellation targeted an S/N of 50 in F160W, including all pixels within 3 R_e. For instance, in the F098M–F160W color profile, out of 1093 pixels we get 128 binned tiles. Figure 3 shows both color profiles from the WFC3/IR data, with the corresponding rest-frame $U - V$ and $B - V$ colors on the right axes (the K-corrections were computed for a range of SSPs at solar metallicity). We note that an analysis of the deconvolved images gives no significant difference, confirming that the change with respect to the PSF for the three WFC3/IR passbands used introduces no significant biases in the colors. Within the core ($R \lesssim R_e$) the colors are slightly bluer than in the outer regions, but still around $(U - V)_0 \sim 1$, reflecting either small levels of ongoing star formation or dust reddening. The following section presents the spectroscopic analysis that provides more stringent constraints on the underlying stellar populations.

4. MODELLING THE STAR FORMATION HISTORY

The high S/N of the WFC3-IR slitless grism data allows us to perform the fitting of the spectral energy distribution (SED) corresponding to the rest-frame 3500–5500 Å, i.e., a region very sensitive to the age and metallicity distribution. We note that a contaminant spike is present in the original WFC3 SED at an observed $\lambda = 15100$ Å. At the redshift of the galaxy, this contamination appears very close to the metallicity-sensitive Mg I region around 5170 Å (see Figure 3 of van Dokkum & Brammer 2010). In order to be able to use this region, we corrected it by running the CST models (described below), fitting the spectrum over the wavelength range 3500–5100 Å. The best fit (extended to 5500 Å) is then used to perform a correction in the region of the spike—which extends over ∼200 Å, redward of the Mg I feature. We tested our results in the two cases, i.e., without any correction, fitting only blueward of 5100 Å, and with the correction, fitting out to 5500 Å, to find no significant difference in the age distributions, but an important suppression of the probability distribution toward very low metallicities.

The spectrum (shown in Figure 1) shows prominent Balmer lines, characteristic of stellar populations of ages around 1 Gyr. We used the ACS data to measure the MgUV feature (a local peak in the heavily blanketed NUV continuum at rest-frame 2625–2725 Å) and obtained a value of MgUV $= 1.16 \pm 0.04$, which is also indicative of a similar age (see, e.g., Figure 2 in Daddi et al. 2005). Our aim in this section is to characterize the past SFH of FW4871. The discovery paper of this system (van Dokkum & Brammer 2010) already presented a first approach to this problem, using the method outlined in Kriek et al. (2009). In this paper we explore in more detail this issue, including additional information from the MgUV feature and determine robust uncertainties on the derived formation history by the use of a large number of models. We ran four separate grids of models, as outlined below. For each choice of the SFH, we define a likelihood combining—as independent observables—the WFC3 spectral data, the measured colors (F098M–F1609W and F125W–F160W), and the MgUV index obtained from the ACS spectrum. Note that we have two separate runs for a WFC3 extraction of 3 and 5 pixels, corresponding to diameters of 0.38 and 0.64 arcsec, respectively. The ACS and photometric data are extracted to match the same apertures (see Table 1 for the values used). The best fits obtained for these models are shown in Table 2.

Table 2
Parameter Fits, Combining the WFC3/IR SED, the MgUV Index (Measured from the ACS SED), and F098M, F125W, and F160W Photometry

Model	PopSyn	Aperture	⟨Age⟩ (Gyr)	Δt (Gyr)	$\log Z/Z_\odot$	$E(B-V)$	$\log M_s/M_\odot$	$\chi^2_{r,min}$
Calzetti Reddening (Calzetti 2001)								
SSP	BC07	0.″38	$0.77^{+0.06}_{-0.06}$	...	$-0.58^{+0.04}_{-0.08}$	<0.02	$11.33^{+0.04}_{-0.04}$	1.36
SSP	BC07	0.″64	$0.88^{+0.07}_{-0.14}$	...	$-0.60^{+0.06}_{-0.07}$	<0.02	$11.36^{+0.07}_{-0.06}$	1.45
SSP	CM05	0.″38	$0.77^{+0.06}_{-0.05}$	...	$-1.33^{+0.07}_{-0.03}$	<0.02	$10.69^{+0.04}_{-0.04}$	3.31
SSP	CM05	0.″64	$0.80^{+0.06}_{-0.06}$	...	$-1.21^{+0.08}_{-0.04}$	<0.02	$10.69^{+0.04}_{-0.04}$	3.58
EXP	BC07	0.″38	$0.63^{+0.10}_{-0.11}$	$0.17^{+0.02}_{-0.03}$	$+0.21^{+0.03}_{-0.08}$	$0.06^{+0.04}_{-0.05}$	$11.45^{+0.03}_{-0.03}$	1.02
EXP	BC07	0.″64	$0.67^{+0.11}_{-0.07}$	$0.17^{+0.03}_{-0.01}$	$+0.20^{+0.03}_{-0.10}$	$0.05^{+0.03}_{-0.04}$	$11.45^{+0.07}_{-0.04}$	1.11
EXP	CM05	0.″38	$0.45^{+0.05}_{-0.10}$	$0.12^{+0.03}_{-0.02}$	$+0.21^{+0.03}_{-0.08}$	<0.04	$10.74^{+0.03}_{-0.03}$	1.78
EXP	CM05	0.″64	$0.47^{+0.19}_{-0.05}$	$0.15^{+0.04}_{-0.02}$	$+0.20^{+0.04}_{-0.12}$	$0.02^{+0.02}_{-0.01}$	$10.75^{+0.08}_{-0.04}$	2.10
CST	BC07	0.″38	$1.44^{+0.10}_{-0.24}$	$2.71^{+0.12}_{-0.41}$	$+0.21^{+0.03}_{-0.03}$	$0.05^{+0.02}_{-0.01}$	$11.59^{+0.04}_{-0.07}$	0.88
CST	BC07	0.″64	$1.46^{+0.08}_{-0.17}$	$2.76^{+0.07}_{-0.37}$	$+0.21^{+0.03}_{-0.05}$	$0.06^{+0.02}_{-0.01}$	$11.60^{+0.03}_{-0.03}$	1.03
CST	CM05	0.″38	$0.73^{+0.12}_{-0.15}$	$1.43^{+0.08}_{-0.29}$	$+0.21^{+0.03}_{-0.03}$	$0.03^{+0.02}_{-0.02}$	$10.82^{+0.03}_{-0.03}$	1.57
CST	CM05	0.″64	$0.78^{+0.11}_{-0.15}$	$1.47^{+0.26}_{-0.11}$	$+0.21^{+0.03}_{-0.06}$	$0.05^{+0.02}_{-0.01}$	$10.82^{+0.06}_{-0.04}$	1.86
Milky Way Reddening (Fitzpatrick 1999)								
SSP	BC07	0.″38	$0.77^{+0.06}_{-0.06}$	...	$-0.58^{+0.04}_{-0.08}$	<0.02	$11.33^{+0.04}_{-0.04}$	1.36
SSP	BC07	0.″64	$0.89^{+0.06}_{-0.09}$	...	$-0.60^{+0.06}_{-0.07}$	<0.02	$11.36^{+0.07}_{-0.06}$	1.45
SSP	CM05	0.″38	$0.77^{+0.06}_{-0.06}$	...	$-1.32^{+0.08}_{-0.03}$	<0.02	$10.68^{+0.04}_{-0.04}$	3.31
SSP	CM05	0.″64	$0.81^{+0.06}_{-0.06}$	...	$-1.21^{+0.08}_{-0.04}$	<0.02	$10.68^{+0.04}_{-0.04}$	3.58
EXP	BC07	0.″38	$0.63^{+0.11}_{-0.11}$	$0.17^{+0.01}_{-0.03}$	$+0.21^{+0.03}_{-0.07}$	$0.02^{+0.03}_{-0.02}$	$11.44^{+0.03}_{-0.03}$	1.02
EXP	BC07	0.″64	$0.72^{+0.09}_{-0.10}$	$0.17^{+0.03}_{-0.02}$	$+0.20^{+0.03}_{-0.13}$	$0.02^{+0.03}_{-0.02}$	$11.44^{+0.03}_{-0.03}$	1.14
EXP	CM05	0.″38	$0.46^{+0.04}_{-0.04}$	$0.13^{+0.03}_{-0.02}$	$+0.21^{+0.03}_{-0.08}$	<0.02	$10.74^{+0.03}_{-0.03}$	1.78
EXP	CM05	0.″64	$0.50^{+0.26}_{-0.08}$	$0.16^{+0.05}_{-0.02}$	$+0.12^{+0.11}_{-0.08}$	$0.02^{+0.01}_{-0.02}$	$10.77^{+0.07}_{-0.06}$	2.13
CST	BC07	0.″38	$1.39^{+0.14}_{-0.23}$	$2.46^{+0.36}_{-0.33}$	$+0.21^{+0.03}_{-0.03}$	$0.03^{+0.01}_{-0.02}$	$11.55^{+0.06}_{-0.06}$	0.92
CST	BC07	0.″64	$1.44^{+0.10}_{-0.27}$	$2.68^{+0.15}_{-0.51}$	$+0.15^{+0.05}_{-0.64}$	$0.06^{+0.01}_{-0.06}$	$11.58^{+0.04}_{-0.08}$	1.09
CST	CM05	0.″38	$0.78^{+0.07}_{-0.15}$	$1.46^{+0.05}_{-0.12}$	$+0.21^{+0.03}_{-0.06}$	$0.02^{+0.02}_{-0.01}$	$10.81^{+0.03}_{-0.03}$	1.60
CST	CM05	0.″64	$1.25^{+0.26}_{-0.50}$	$2.56^{+0.26}_{-1.13}$	$+0.21^{+0.03}_{-0.18}$	<0.04	$10.89^{+0.09}_{-0.08}$	1.97

Notes. Ages are defined as mass-weighted values. For the EXP models, the age dispersion Δt is defined as the rms of the distribution; for CST models it represents the duration of the burst. Error bars are quoted at the 5–95 percentiles.

4.1. Simple Stellar Populations

A first approach would involve SSPs, defined by a single age and metallicity. We also include dust as a free parameter described by $E(B-V)$, modifying the spectrum with two reddening laws: the Calzetti (2001) law—appropriate for starbursting systems—and a Milky Way reddening law (Fitzpatrick 1999). The grid of model parameters is defined in Table 3. Figure 4 shows the confidence levels on age and metallicity, marginalized over dust, for two population synthesis models: the 2007 version of the Bruzual & Charlot (2003) models (Bruzual 2007, hereafter BC07), and those of Maraston (2005, hereafter CM05). Each panel in Figure 4 corresponds to one of the two extractions, as defined above (other results are shown in Table 2, with the uncertainties given at the 5 and 95 percentiles). Note the significant difference with respect to stellar mass between BC07 and CM05 models, a well-known feature caused by the different prescriptions included in these models, most notably the modeling of the TP-AGB phase (Maraston et al. 2006). The insets show the cumulative probability distribution of dust, which shows good agreement between both models, with values below $E(B-V)=0.02$ at the 95% confidence level. Given the merger-like morphology of the object (Figure 2), it is quite remarkable to obtain such a low level of dust and a relatively "old" SSP-age (the presence of ongoing star formation would shift the derived age to lower values). However, it is a well-known fact that SSP-based fits are not robust indicators of age unless we are dealing with a system formed over a short period of time compared to stellar evolution timescales (e.g., a globular cluster), or for systems with old and early truncated SFHs (e.g., a massive early-type galaxy, see Rogers et al. 2010). Note that the best-fit SSP gives a rather low metallicity, especially for the CM05 models. The constraint on a single age to explain a composite population can result in such values on the metallicity. To overcome this, we consider more realistic composite models where the SFH is parameterized by a small number of variables. A different reddening law does not change the outcome, a result that will be consistent for the composite models. The reason is that the reddening law used in this analysis pertains mainly to the optical region, where most reddening laws do not differ much. In the NUV, the only information used—the MgUV index—is rather immune to a change in reddening law given that it is defined over a small spectral window, and it is located away from the "2175 Å bump" (see, e.g., Conroy et al. 2010).

4.2. Exponential Models

The lack of signatures of ongoing star formation in the SED of FW4871 argues against an exponentially decaying star formation rate. However, these models have been commonly applied to evolved stellar populations, and so we present as

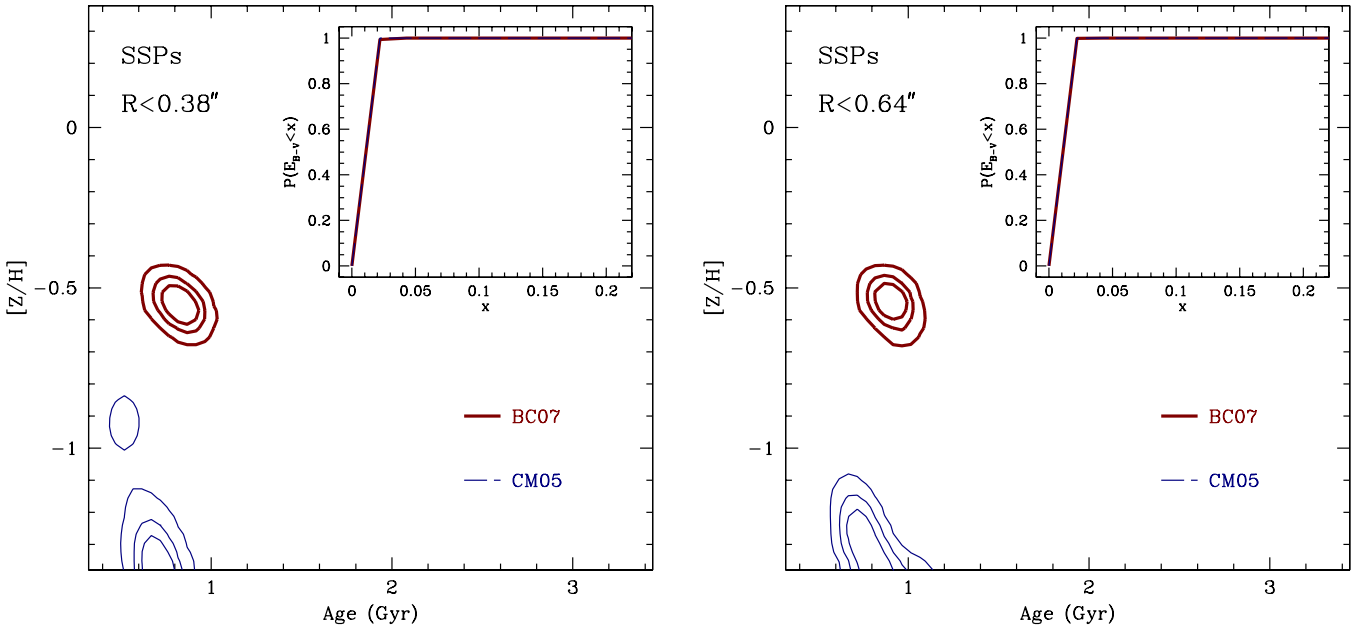

Figure 4. Contours show the 69%, 90%, and 99% confidence levels for the spectral fitting of the WFC3 (rest-frame optical) and the ACS data (rest-frame NUV). In this case the models used are simple stellar populations (i.e., a single age and metallicity), including dust as a free parameter. The inset shows the cumulative distribution of dust. We compare the 2007 version of the Bruzual & Charlot (2003) models with the models of Maraston (2005), as labeled. Two SED extractions of the WFC3 data are considered: a 3 pixel one (left, labeled $R < 0\farcs38$, corresponding to a physical extent of 3.2 kpc) and a 5 pixel extraction (right, labeled $R < 0\farcs64$, corresponding to 5.4 kpc).

(A color version of this figure is available in the online journal.)

Table 3
List of Parameters used in the Models Explored in this Paper

Model	Parameter	Range	Description	No. of Models
SSP	$z_{\rm FOR}$,$t_{\rm FOR}$	[10,$z_{\rm obs}$]	Formation epoch (single age)	
	$\log(Z/Z_\odot)$	[−1.5,+0.3]	Metallicity	
	$E(B-V)$	[0,0.5]	Dust reddening	
				262,144
EXP	$z_{\rm FOR}$,$t_{\rm FOR}$	[10,$z_{\rm obs}$]	Formation epoch	
	$\log(\tau/{\rm Gyr})$	[−1,+0.6] Gyr	Formation timescale	
	$\log(Z/Z_\odot)$	[−1.5,+0.3]	Metallicity	
	$E(B-V)$	[0,0.5]	Dust reddening	
				1,048,576
CST	$z_{\rm FOR}$,$t_{\rm FOR}$	[10,$z_{\rm obs}$]	Formation epoch	
	Δt	[0,$(t_U - t_{10}) \sim 3$] Gyr	Burst duration	
	$\log(Z/Z_\odot)$	[−1.5,+0.3]	Metallicity	
	$E(B-V)$	[0,0.5]	Dust reddening	
				1,048,576
CST2	$z_{\rm FOR}$,$z_{\rm FOR}$	10	Formation epoch (fixed)	
	Δt	[0,$(t_U - t_{10}) \sim 3$] Gyr	Burst duration	
	$E_O(B-V)$	[0,0.5]	Dust reddening (old)	
	t_Y	[0.1,2] Gyr	Young component (SSP)	
	$E_Y(B-V)$	[0,0.5]	Dust reddening (young)	
	f_Y	[0,1]	Young stellar mass fraction	
	$\log(Z/Z_\odot)$	[−1.5,+0.3]	Metallicity (both components)	
				2,985,984

Notes. A formation time or epoch can be given either by a cosmological time ($t_{\rm FOR}$) or by the corresponding redshift ($z_{\rm FOR}$). t_U and t_{10} represent the age of the universe at the redshift of FW4871 ($z_{\rm obs} = 1.893$) and the cosmological time at redshift $z = 10$, respectively.

an exercise the results of fitting such models (hereafter EXP models), whereby four parameters describe an SFH, namely the formation epoch ($t_{\rm FOR}$, the cosmic epoch when star formation starts), the timescale of the exponential (τ), the metallicity (Z, kept fixed for all times within a model), and the dust content, parameterized by the color excess $E(B-V)$. These so-called τ-models improve over the SSPs as they consist of a mixture of stellar ages, giving a more realistic representation of the real SFH, with τ controlling the width of the age distribution. Table 3 shows the range explored for these parameters. Table 2 lists the parameter fits, including the average age and the rms of the age distribution (using the likelihood as the probability distribution

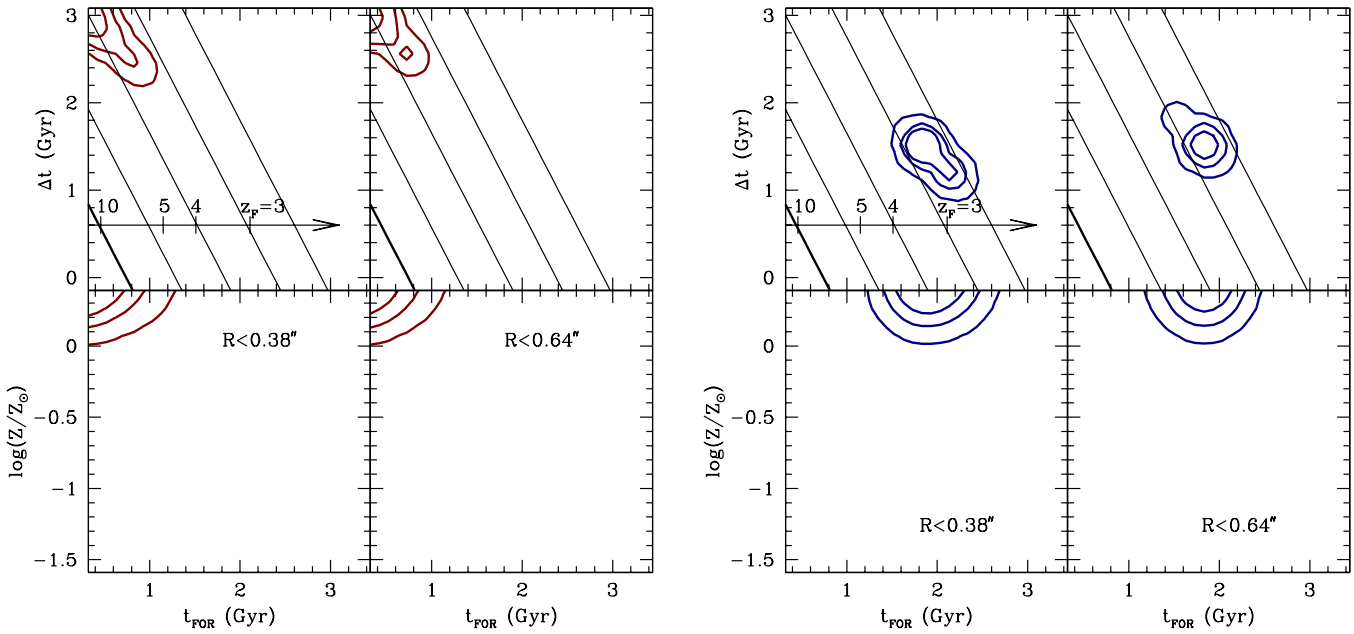

Figure 5. As in Figure 4 for the fit from the truncated models (CST, see text for details). The panels on the left (right) correspond to the BC07 (CM05) models. The top panels also show the contours for an mass-weighted average age from 0.5 Gyr to 2.5 Gyr (thick line) in steps of 0.5 Gyr. The composite models are based on the population synthesis models of BC07 (left) and CM05 (right).

(A color version of this figure is available in the online journal.)

function of the parameter considered). The average mass-weighted stellar age according to EXP models lies between 0.5 and 0.7 Gyr, depending on the population synthesis library used. We note that the age of the universe at the redshift of FW4871 is 3.4 Gyr. The main difference between the BC07 and CM05 models is the lower value of the age for the latter. Nevertheless, both population synthesis models agree with a rather unphysical short-lived burst of formation ($\tau < 0.2$ Gyr). In contrast to the SSP runs, solar and super-solar abundances are now allowed, and the best-fit χ^2 values are significantly reduced. These models would suggest that the bulk of the stellar populations of FW4871 were formed in an intense and very short lived burst started at redshift $z_F \sim 2.5$–3.

4.3. Truncated Models

There is an important limitation with exponentially decaying models: the tail of the exponential creates a small, but significant amount of very young stars. The flux from those stars will affect the spectral fit considerably. Hence, it is necessary—for spectra without a significant amount of star formation—to adopt an additional set of models, namely those where the star formation is truncated. For simplicity, we assume that the star formation rate is constant within an interval between cosmic time $t_{\rm FOR}$ and $t_{\rm FOR} + \Delta t$, and then switches abruptly to zero (hereafter, we refer to this set as CST models). This parameterization allows us to get a more realistic estimate of the duration of the burst if no young stars are found in the spectra (as suggested, e.g., by the color distribution, the SSP fits of the spectra, or the absence of strong emission lines). Dust is also included as a free parameter in the same way as for the SSP and EXP models. Once again, Table 3 shows the range explored for these models. Figure 5 shows the confidence levels for these models, using the same observational constraints as for the EXP and the SSP models. The figure gives the constraints on the parameters controlling the age (top) and metallicity (bottom). The slanted lines in the top panels represent an average, mass-weighted age between 0.5 and 2.5 Gyr (thick line), in steps of 0.5 Gyr. Note the degeneracy between age and burst duration is reduced for the analysis with the BC07 models (left panels). The CM05 models allow for the presence of younger stars, but the χ^2 are slightly worse than for the BC07-based models.

The figure suggests an average age of about 1.5 Gyr, with a wide age spread, between 2–3 Gyr, and metallicities above $Z_\odot/3$. The results do not vary significantly with respect to the choice of the 0.″38 ($\sim R_e/2$) or 0.″64 ($\sim R_e$) diameter apertures considered, suggesting rather homogeneous stellar populations.

4.4. Beyond Truncated Models

One could argue that the single dust screen, adopted for our models so far, may not take into account a more complex SFH. Complex models come at the price of huge volumes of parameter space. Furthermore, the inherent degeneracies present in any analysis of stellar populations from unresolved spectroscopic data lead us to follow the approach of mapping as much as possible the full volume of parameter space. Hence, in order to constrain the presence of a younger population, *with different dust reddening* from the rest of galaxy, we define a new set of models (CST2) consisting of the previous one, i.e., constant star formation truncated after some time lapse Δt, along with an extra component made up of a young SSP. In order to make the parameter search manageable, we assume a formation epoch for the old component of $z_{\rm FOR} = 10$ and assume the same metallicity for both components (although allowed to be a free parameter). Hence, this model is described by six free parameters (see Table 3). The new parameters describe the age of the young component (t_Y), its contribution in mass (f_Y), and the amount of dust in the old and young components (E_O and E_Y). Given the small differences found with respect to attenuation laws, we will only consider a standard Fitzpatrick (1999) law for CST2 models.

Figure 6 shows the constraints on the parameters mainly related to the young component (we do not find significant

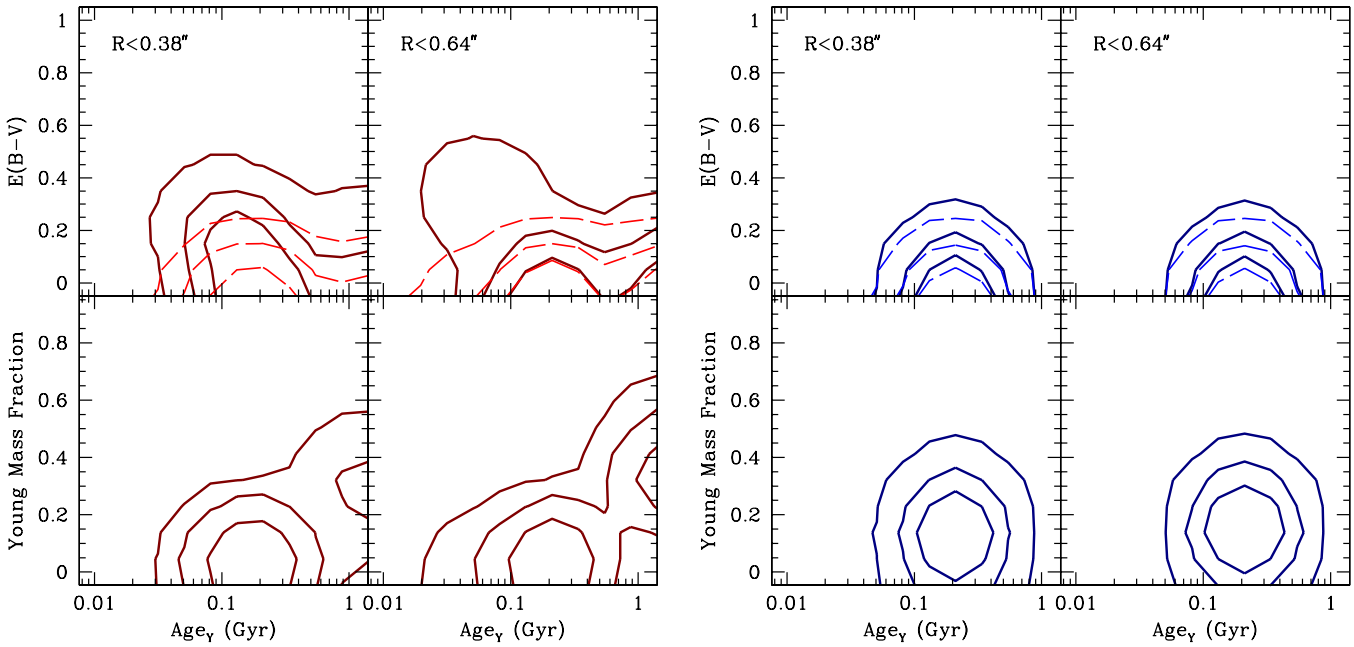

Figure 6. Contours are shown at the 69%, 90%, and 99% confidence levels for the fit corresponding to the truncated models plus a later burst in the form of a simple stellar population (CST2; see text for details). The figure shows the properties of the secondary (younger) component, as labeled. The older component features similar constraints to the CST models shown above (i.e., Figure 5). In the top panels we show the constraints for the independent dust reddening parameters of the old (dashed lines) and the young (solid lines) components. The composite models are based on the population synthesis models of BC07 (left) and CM05 (right).

(A color version of this figure is available in the online journal.)

Table 4

Parameter Fits for the CST2 Models, Combining the WFC3/IR SED, the MgUV Index (Measured from the ACS SED), and F098M, F125W, and F160W Photometry

PopSyn	Aperture	⟨Age⟩ (Gyr)	Δt (Gyr)	log (t_Y/Gyr)	f_Y	E_Y ($B-V$)	log $Z/Z_\odot$	log $M_s/M_\odot$	$\chi^2_{r,min}$
BC07	0.″38	$1.55^{+0.25}_{-0.19}$	$2.37^{+0.27}_{-0.75}$	$-0.85^{+0.62}_{-0.30}$	$0.06^{+0.26}_{-0.06}$	<0.21	$+0.22^{+0.08}_{-0.08}$	$11.47^{+0.13}_{-0.13}$	0.58
BC07	0.″64	$1.76^{+0.20}_{-0.40}$	$1.99^{+0.56}_{-0.34}$	$-0.83^{+0.09}_{-0.45}$	$0.06^{+0.26}_{-0.06}$	<0.28	$+0.21^{+0.08}_{-0.08}$	$11.47^{+0.13}_{-0.13}$	0.65
CM05	0.″38	$1.86^{+0.85}_{-0.50}$	$1.15^{+1.18}_{-1.09}$	$-0.82^{+0.08}_{-0.08}$	$0.13^{+0.10}_{-0.10}$	<0.10	$+0.15^{+0.13}_{-0.16}$	$10.89^{+0.14}_{-0.26}$	0.97
CM05	0.″64	$1.94^{+0.23}_{-0.21}$	$1.72^{+0.41}_{-0.46}$	$-0.82^{+0.08}_{-0.08}$	$0.14^{+0.09}_{-0.05}$	<0.10	$+0.18^{+0.11}_{-0.18}$	$10.90^{+0.13}_{-0.13}$	1.12

Notes. For ease of comparison with CST models, ⟨Age⟩ is defined here as the average age of the older component. Error bars are quoted at the 5–95 percentiles.

differences for the parameters controlling the old component, i.e., the equivalent of Figure 5 for the CST2 models would be very similar). On the top panels of Figure 6, the amount of dust reddening is shown both for the old (thin lines) and the young component (thick lines). Table 4 shows the parameter fits over the 5–95 percentiles. Note that the minimum value of the χ^2 decreases—although we must emphasize that all models explored here give acceptable fits, so that a Bayesian evidence criterion would not be capable of discriminating among these models. Nevertheless, the CST2 models show that a young component could be present, although with an age of 145^{+450}_{-70} Myr, and a maximum amount of dust reddening of $E(B-V) < 0.4$ mag (95% confidence levels). Its contribution to the total stellar mass budget changes slightly with respect to the aperture or the population synthesis models used, but stays roughly below 20% for all models, with a best-fit value in the range 5%–15%.

Figure 7 shows the comparison between the observed and the best-fit WFC3 spectra for the BC07 and CM05 models, as black and gray lines, respectively. As regards emission lines, [O II] is only a 1σ residual in the 0.38 arcsec extraction, increasing to 2σ in the larger aperture. Hβ is more prominent, at the 2σ–2.5σ level in the CM05 case. However, we note that FW4871 has an X-ray source counterpart (Luo et al. 2008) and the implied X-ray luminosities could not be expected from a starbursting system unless rates as high as 1000 $M_\odot$ yr^{-1} are sustained, leaving us with the option of an active galactic nucleus (AGN; van Dokkum & Brammer 2010) in an otherwise gas-poor merger. Alternatively, one could consider the X-ray emission originating from a hot, diffuse halo. This X-ray halo can be produced by the conversion of gravitational potential energy into heat. As this galaxy went through a major growth phase in its past, it is likely that this process was accompanied by a major growth phase via infall of material, providing gravitational potential energy. In this way, star formation could have continued until the halo was heated up to sufficiently high temperatures. Khochfar & Ostriker (2008) find that the fastest growing halos would also heat the most. In this case, the residuals found could indeed be related to some (low-level) ongoing star formation (although note the lack of blue colors in Figure 3). During the runs we also compute the absolute luminosity and the $U-V$ color for each SFH. It is worth noting that the best-fit models consistently

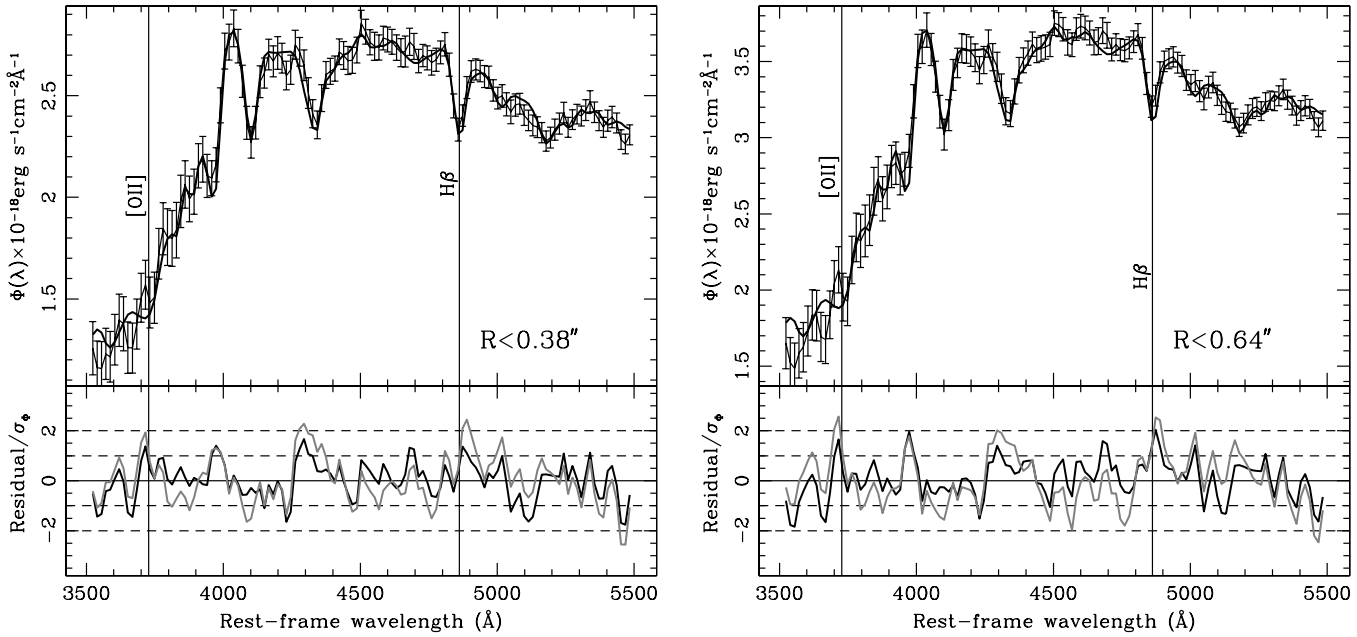

Figure 7. Best fit of the WFC3 slitless grism data for the CST2 models shown in the rest frame, with each panel showing a different extraction, as labeled. The residuals (as a fraction of the rms per wavelength bin) are shown in the bottom panel. The black (gray) lines correspond to the fits using the BC07 (CM05) models.

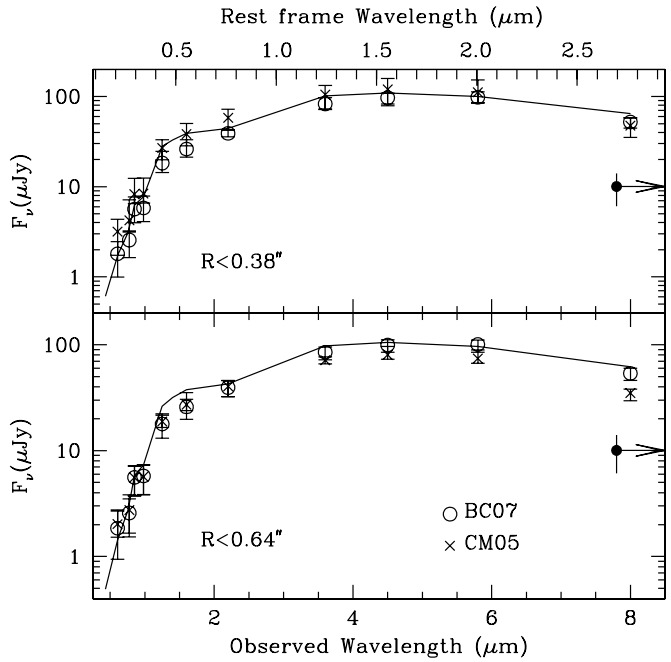

Figure 8. Photometric SED corresponding to the results from the spectroscopic fits. The points represent the probability weighted fluxes according to the CST2 models, with error bars extending over the 90% confidence interval. The line shows the photometric data from *HST*/ACS, VLT/ISAAC, *HST*/WFC3-IR, and *Spitzer*/IRAC. The solid dot with an arrow marks the observed frame 24 μm flux from *Spitzer*/MIPS (taken from Wuyts et al. 2008).

give a luminosity of $M_V = -24.89 \pm 0.07$ and a color $U - V = 1.3 \pm 0.06$ (AB, 90% confidence levels) regardless of the model or base population synthesis.

As a final check of our (mainly spectroscopic) fits with respect to broadband photometry, covering a wider range of wavelengths, we show in Figure 8 a comparison between the observed photometric data and the best-fit CST2 models obtained from spectral fitting. The observations are given in the figure as a solid line, whereas the model fits are shown as open circles (BC07) or crosses (CM05), with error bars representing the 90% confidence levels. The observations cover a wide range, from the optical (*HST*/ACS) to the IR (*Spitzer*/IRAC), including NIR (VLT/ISAAC and *HST*/WFC3-IR). Note the constraint from spectral fitting only uses data out to $\lambda_{obs} \sim 1.6\,\mu$m, whereas the photometric SED shown here as a solid line comes from the total fluxes (taken from the FIREWORKS survey; Wuyts et al. 2008). In the case of the ACS and WFC3 data, we performed aperture photometry on the images, so that those fluxes correspond to the chosen 0.″38 and 0.″64 apertures. The IRAC fluxes cannot be treated this way, given the poorer spatial resolution. The fit is good for most of the photometric data points with BC07 models. In contrast, the CM05-based models give slightly higher NUV fluxes and lower 8 μm fluxes, an aspect that cannot be blamed on dust, since the models give a strong constraint in $E(B - V)$ (see Tables 2 and 4). An increase in the amount of dust would drastically worsen the SED fitting of the WFC3 data, whose superb flux calibration cannot accommodate larger amounts of reddening. The relatively weak flux observed in the 24 μm *Spitzer*/MIPS passband ($\Phi_{24} = 10.05\,\mu$Jy, compared with an 8 μm flux of $\Phi_8 = 62.0\,\mu$Jy; Wuyts et al. 2008) confirms that emission from dust—and thus significant star formation—is rather low in this galaxy.

5. DISCUSSION AND CONCLUSIONS

FW4871 constitutes a typical case of a massive galaxy already in place by redshift $z \sim 2$. This type of galaxy is expected to evolve into the massive early-type galaxies we see at low redshift. Taking the redshift catalog from the ESO database (Popesso et al. 2009; Balestra et al. 2010) we find 13 (54) galaxies within a redshift range $1.8 < z < 2.0$ at a projected separation below ± 1 (2) Mpc. Hence, regarding environment—over the large scales mapped by this redshift range—this galaxy clearly sits in an overdense region.

We find that a realistic model consisting of a truncated SFH gives no significant star formation in the recent past history of FW4871, whereas the duration of the bursting episode extends for around 2.5 Gyr. Unfortunately, the best-fit values of the likelihood (i.e., the "minimum χ^2") are similar among sets of models, preventing us to discriminate among SSP, EXP, CST, CST2, or other sets of models using, for instance, a Bayesian evidence estimator, even with better spectral resolution (see Rogers et al. 2010 for a detailed analysis in low-redshift galaxies). One can only resort to prior information in the sense of rejecting models such as an SSP, where the formation takes place over a timescale much shorter than the dynamical timescales of the systems concerned, or EXP models, where a protracted tail of star formation is at odds with the lack of line emission related to ongoing star formation. Nevertheless, all models point to the fact that no significant star formation took place during the latest stages of FW4871, at least within one effective radius. Furthermore, the color profile of this galaxy (Figure 3) suggests a similar outcome in the external regions, out to 3 R_e.

We emphasize that within the 4.65 arcmin^2 field of view of the ERS/GOODS data, FW4871 is the only galaxy with a strong Balmer decrement observed in the redshift range sensitive to the WFC3 grism data (i.e., $1 < z < 3$). Given the limit in apparent magnitude of the observations, this constraint is compatible with the comoving number density of massive galaxies at $z \sim 2$ ($n \sim 10^{-4}$ Mpc^{-3}; Conselice et al. 2007). Is FW4871 an outlier or a typical example of a forming massive galaxy? Larger surveys to a comparable depth are needed to answer this question.

The analysis of FW4871 by van Dokkum & Brammer (2010) compared the WFC3-IR spectrum with a small set of synthetic spectra, proposing a stellar age of 0.5 Gyr and $A_V \sim 1$ mag, with a tentative, although very weak, detection of Hβ in emission in the outer regions of the galaxy. Their spectral fit only presented three possible SFHs, without any reference to the range of models explored. Hence, their suggested scenario cannot include an estimate of uncertainty in the properties of the underlying stellar populations. In addition, we note that van Dokkum & Brammer (2010) extracted the data from the publicly available server and performed the reduction of the data while the latest calibration files were not available. Our team used the best possible calibration files, obtaining a slightly different SED compared to the one presented in van Dokkum & Brammer (2010), hence the difference with respect to the dust content. Even though the simple scenarios presented in their paper are compatible with our analysis regarding age, their estimate of dust cannot be accommodated with the spectrum reduced with the newest calibration data.

We extend the analysis of van Dokkum & Brammer (2010) by exploring a wide range of SFHs, and include the color gradients to strengthen the hypothesis that the star formation in FW4871 has been truncated in the recent past of its history. The main conclusion from our analysis of the stellar populations within the effective radius is that the process of formation started at redshift $z_F \sim 10$ and lasted for about ~2.5 Gyr. The addition of an extra, younger component to the analysis allows for up to 20% in mass of a population with an age of ~150 Myr, with a modest amount of dust reddening ($E(B-V) < 0.4$ mag), therefore with the bulk of stellar populations having formed at an earlier phase. The long Δt of the models along with the lack of star-forming features in the spectrum suggests a truncation of the star formation over a few hundreds of Myr. Taking into account the stellar mass of the galaxy, we can infer a sustained star formation rate during its bursting phase in the range 30–110 $M_\odot$ yr^{-1} (with the quoted range including the difference between the stellar masses according to the BC07 or CM05 models). One expects the star-forming progenitors to be similar to SCUBA galaxies (see, e.g., Chapman et al. 2005), at $z \gtrsim 2.5$. FW4871 represents the endpoint of the strong star formation activity of a massive galaxy, perhaps followed by a number of minor mergers—such as the one expected with its neighbor FW4887—that will increase its compact size toward those of local massive galaxies (Khochfar & Silk 2006a; Naab et al. 2009). Regarding the discrepancy in the stellar mass given by either the BC07 or CM05 models, we note that this disagreement is caused by the difference in the treatment of evolved phases of stellar evolution, with TP-AGB stars contributing significantly more to the luminosity in the CM05 models, thereby reducing the M/L especially for the ages considered. However, we note that this predicted contribution still awaits confirmation by observations (e.g., Zibetti et al. 2012).

Given the mass of this galaxy, one should expect a major contribution to its formation via cold accretion at high redshift (see, e.g., Dekel & Birnboim 2006), a process that would boost the star formation rate both from the enhanced gas accretion rate and a possible increase of the star formation efficiency (see, e.g., Khochfar & Silk 2009). The derived SFH of FW4871 provides evidence—via the superb spectroscopic data from *HST*—toward a highly efficient channel of galaxy formation that started around $z_F \sim 10$, and was subsequently truncated around $z \gtrsim 2$, followed by a brief quiescent phase. What caused this truncation? Two main scenarios can be brought forward. (1) The onset of a galactic superwind from stellar feedback: a sustained star formation rate of about ~100 $M_\odot$ yr^{-1} for a couple of Gyr will provide enough energy. (2) The previous merging process that resulted in the formation of FW4871 could be the ultimate cause of the quenching, possibly by switching of the AGN (Hambrick et al. 2011). The morphological appearance of FW4871, and the X-ray detection of this source (Luo et al. 2008), points to the latter. In this case, the recent merging process to form FW4871 could be considered as the cause of truncation. One could envision FW4871 as a high-redshift equivalent of a post-starburst, or k+a galaxy. The analysis of the environment in a sample of k+a galaxies from the Sloan Digital Sky Survey (Goto 2005) reveals that the truncation of the starbursting phase is caused by the interaction with a nearby companion, a similar mechanism to the one contemplated here.

This process would make major mergers an important factor to explain the "road to the red sequence," namely, the process of quenching of star formation in massive galaxies, an issue that may require proper calibration of semi-analytic models of galaxy formation.

We gratefully acknowledge enlightening discussions with Daisuke Kawata and Myrto Symeonidis. We made extensive use of the Delos Computer Cluster in the Physics Department at King's College London, with thanks to the sysadmin Dr. Nigel Arnot.

Facility: HST (ACS,WFC3)

REFERENCES

Baldry, I. K., Glazebrook, K., Brinkmann, J., et al. 2004, ApJ, 600, 681
Balestra, I., Mainieri, V., Popesso, P., et al. 2010, A&A, 512, 12
Balogh, M. L., Morris, S. L., Yee, H. K. C., Carlberg, R. G., & Ellingson, E. 1999, ApJ, 527, 54
Banerji, M., Ferreras, I., Abdalla, F., Hewet, P., & Lahav, O. 2010, MNRAS, 402, 2264

Bournaud, F., Jog, C. J., & Combes, F. 2007, A&A, 476, 1179
Bruzual, G. 2007, in IAU Symp. 241, Stellar Populations as Building Blocks of Galaxies, ed. A. Vazdekis & R. F. Peletier (Cambridge: Cambridge Univ. Press), 125
Bruzual, G., & Charlot, S. 2003, MNRAS, 344, 1000
Calzetti, D. 2001, PASP, 113, 1449
Chapman, S. C., Blain, A. W., Smail, I., & Ivison, R. J. 2005, ApJ, 622, 772
Cimatti, A., Cassata, P., Pozzetti, L., et al. 2008, A&A, 482, 21
Conroy, C., Schiminovich, D., & Blanton, M. R. 2010, ApJ, 718, 184
Conselice, C. J., Bundy, K., Trujillo, I., et al. 2007, MNRAS, 381, 962
Daddi, E., Renzini, A., Pirzkal, N., et al. 2005, ApJ, 626, 680
Damjanov, I., McCarthy, P. J., Abraham, R. G., et al. 2009, ApJ, 695, 101
Dekel, A., & Birnboim, Y. 2006, MNRAS, 368, 2
Dekel, A., Birnboim, Y., Engel, G., et al. 2009, Nature, 457, 451
Dressler, A., & Gunn, J. E. 1992, ApJS, 78, 1
Fan, L., Lapi, A., De Zotti, G., & Danese, L. 2008, ApJ, 689, L101
Ferreras, I., Lisker, T., Carollo, C. M., Lilly, S. J., & Mobasher, B. 2005, ApJ, 635, 243
Ferreras, I., Lisker, T., Pasquali, A., Khochfar, S., & Kaviraj, S. 2009a, MNRAS, 396, 1573
Ferreras, I., Pasquali, A., Malhotra, S., et al. 2009b, ApJ, 706, 158
Ferreras, I., & Yi, S. K. 2004, MNRAS, 350, 1322
Fitzpatrick, E. L. 1999, PASP, 111, 63
Fontana, A., Salimbeni, S., Grazian, A., et al. 2006, A&A, 459, 745
Goto, T. 2005, MNRAS, 357, 937
Hambrick, D. C., Ostriker, J. P., Naab, T., & Johansson, P. H. 2011, ApJ, 738, 16
Kauffmann, G., Heckman, T. M., White, S. D. M., et al. 2003, MNRAS, 341, 54
Kereš, D., Katz, N., Fardal, M., Davé, R., & Weinberg, D. H. 2009, MNRAS, 395, 160
Khochfar, S., & Ostriker, J. P. 2008, ApJ, 680, 54
Khochfar, S., & Silk, J. 2006a, MNRAS, 370, 902
Khochfar, S., & Silk, J. 2006b, ApJ, 648, L21
Khochfar, S., & Silk, J. 2009, ApJ, 700, L21
Kriek, M., van Dokkum, P. G., Labbé, I., et al. 2009, ApJ, 700, 221
Kümmel, M., Kuntschner, H., Walsh, J. R., & Bushouse, H. 2010, in ASP Conf. Ser. 434, Astronomical Data Analysis Software and Systems XIX, ed. Y. Mizumoto, K.-I. Morita, & M. Ohishi (San Francisco, CA: ASP), 305
Kümmel, M., Walsh, J. R., Pirzkal, N., Kuntschner, H., & Pasquali, A. 2009, PASP, 121, 59
Longhetti, M., Saracco, P., Severgnini, P., et al. 2007, MNRAS, 374, 614
Lucy, L. B. 1974, AJ, 79, 745
Luo, B., Bauer, F. E., Brandt, W. N., et al. 2008, ApJS, 179, 19
Maraston, C. 2005, MNRAS, 362, 799
Maraston, C., Daddi, E., Renzini, A., et al. 2006, ApJ, 652, 85
Naab, T., Johansson, P. H., & Ostriker, J. P. 2009, ApJ, 699, L178
Nair, P., van den Bergh, S., & Abraham, R. G. 2011, ApJ, 734, L31
Pasquali, A., Ferreras, I., Panagia, N., et al. 2006, ApJ, 636, 115
Peng, C. Y., Ho, L. C., Impey, C. D., & Rix, H.-W. 2010, AJ, 139, 2097
Pérez-González, P. G., Trujillo, I., Barrp, G., et al. 2008, ApJ, 687, 50
Popesso, P., Dickinson, M., Nonino, M., et al. 2009, A&A, 494, 443
Ragone-Figueroa, C., & Granato, G. L. 2011, MNRAS, 414, 3690
Rogers, B., Ferreras, I., Peletier, R., & Silk, J. 2010, MNRAS, 402, 447
Shankar, F., Marulli, F., Bernardi, M., et al. 2010, MNRAS, 403, 117
Spinrad, H., Dey, A., Stern, D., et al. 1997, ApJ, 484, 581
Straughn, A. N., Kuntschner, H., Kümmel, M., et al. 2011, AJ, 141, 14
Trujillo, I., Ferreras, I., & de la Rosa, I. G. 2011, MNRAS, 415, 3903
Trujillo, I., Förster Schreiber, N. M., Rudnick, G., et al. 2006, ApJ, 650, 18
van der Wel, A., Bell, E. F., van den Bosch, F. C., Gallazzi, A., & Rix, H.-W. 2009, ApJ, 698, 1232
van Dokkum, P. G., & Brammer, G. 2010, ApJ, 718, L73
van Dokkum, P. G., Franx, M., Kriek, M., et al. 2008, ApJ, 677, L5
White, S. D. M., & Rees, M. J. 1978, MNRAS, 183, 341
Windhorst, R. A., Cohen, S. H., Hathi, N. P., et al. 2011, ApJS, 193, 27
Wuyts, S., Labbé, I., Schreiber, N. M. F., et al. 2008, ApJ, 682, 985
Zibetti, S., Gallazzi, A., Charlot, S., Pasquali, A., & Pierini, D. 2012, in IAU Symp. 284, The Spectral Energy Distribution of Galaxies, ed. R. J. Tuffs & C. C. Popescu (Cambridge: Cambridge Univ. Press), in press (arXiv:1203.4571)